Supporting Information

# Fast Na-diffusive tin alloy for all-solid-state Na-based batteries

Naoto Tanibata, Koki Matsunoshita, Hirokazu Takeuchi, Suzuno Akatsuka, Misato Koga, Hayami Takeda, Masanobu. Nakayama

All-solid-state Na batteries, which are inexpensive and highly stable, are promising candidates for energy storage in environmentally friendly microgrids and vehicles. Na diffusivity is an important parameter for the performance of these batteries. In this study, we found that the metastable phase $Na_{10}Sn_4$ exhibits fast Na diffusivity (room temperature diffusion coefficient $D_{25}$ = 5.4×10$^{-7}$ cm$^2$ s$^{-1}$), surpassing that of other reported alloys (Sb- and Ge- alloys) as well as oxide and sulfide materials. $Na_{10}Sn_4$ was synthesised by a mechanochemical method, and its electrode properties were evaluated for an all-solid-state battery. The cell exhibited an interfacial resistance of 100.1 Ω cm$^2$, which is smaller than those reported between metallic anodes and solid or liquid electrolytes. These results indicate that $Na_{10}Sn_4$ has significant potential as an ultralow-resistance electrode to improve all-solid-state Na batteries, a major step forward in energy storage materials research.

## Table of Contents



## Experimental Procedures

### Preparation and evaluation of all-solid-state cells using Na–Sn alloy electrodes

Na–Sn alloys ($Na_{10}Sn_4$, $Na_{15}Sn_4$) were synthesised from Na foil (Kanto Chemical Co., Ltd., 99%) and Sn powder (Sigma-Aldrich Japan LLC, 99.9%) using a mechanochemical method. A stoichiometric mixture was placed in a 45 mL stainless steel pot with 10 stainless steel balls (10 mm in diameter) and milled using a planetary ball mill apparatus (Fritsch Japan Co., Ltd., P-7 classic -line) at a rotation speed of 500 rpm for 5 h. Bulk sodium metal was cut, stretched with a hammer, and hollowed with a 6 mmΦ punch to produce the sodium electrodes.

Symmetrical cells were prepared with the following configurations: $Na_{10}Sn_4$ | $Na_3PS_4$ | $Na_{10}Sn_4$, Na metal | $Na_3PS_4$ | Na metal, and $Na_{15}Sn_4$ | $Na_3PS_4$ | $Na_{15}Sn_4$. To achieve this, approximately 70 mg of $Na_3PS_4$ glass-ceramic electrolyte was placed in a hollow, cylindrical polycarbonate insulator with a 10 mmΦ diameter. The insulator was sandwiched by stainless steel and uniaxially pressed at 96 MPa to fabricate the separator pellet. The mass loading of the anode powders was ~10 mg. All-solid-state cells were obtained by placing the appropriate electrodes on both sides and pressing uniaxially at 382 MPa. The applied pressure of the cell during cycling was set to ~50 MPa.

The resulting all-solid-state symmetric cells were subjected to constant-current cycling tests on a potentio-galvanostat (VSP-128, Bio-Logic). The charge–discharge time for each step was 1 h, with a relaxation time of 0.5 h. Current density measurements were conducted for every three charge–discharge cycles. Following each relaxation step, AC impedance measurements were conducted. The applied voltage for the tests was 10 mV, and the frequencies ranged from 0.1 Hz to 1 MHz.

To calculate the diffusion coefficient of $Na_{10}Sn_4$, an all-solid-state battery with a Na counter electrode was fabricated. The constant-current pulse method, which has a shorter measurement time than AC impedance, was used to reduce the effect of the Na electrode degradation. The current value was 64 μA $cm^{-2}$ with an application time of 30 s. All the aforementioned experiments were performed under an argon atmosphere (dew point of approximately <−75 °C, oxygen concentration: 0.0%).

### Evaluation of diffusivity by first-principles MD

First-principles MD calculations based on density functional theory (DFT) were performed to evaluate the Na diffusivity in the Na–Sn alloys. Structures were obtained from The Materials Project ($Na_{10}Sn_4$ mp-1077925, $Na_{15}Sn_4$ mp-30794). Structural optimization was performed via DFT with the generalized density gradient approximation GGA-PBEsol and the Projector-Augmented Wave method using the VASP software. Crystal structure diagrams were drawn using Visualization for Electronic and Structural Analysis (VESTA). The kinetic energy cutoff was 500 eV, and k-point meshes were sampled such that the product of meshes and atoms was approximately 2000. The optimized cell was expanded as a superlattice with a unit lattice approximately six times larger, and a small percentage of Na was removed (~3% $Na_{10}Sn_4$, ~1% $Na_{15}Sn_4$) to create vacancies. In conjunction with constant-current pulse measurements, MD simulations were performed at 298 K for 50 ps at 1 fs per step. The kinetic energy cutoff was 350 eV. Because of limited computational resources, 1 × 1 × 1 k-point sampling was performed. Energy convergence criterion during the iteration was set to $10^{-3}$ eV.

## Results and Discussion

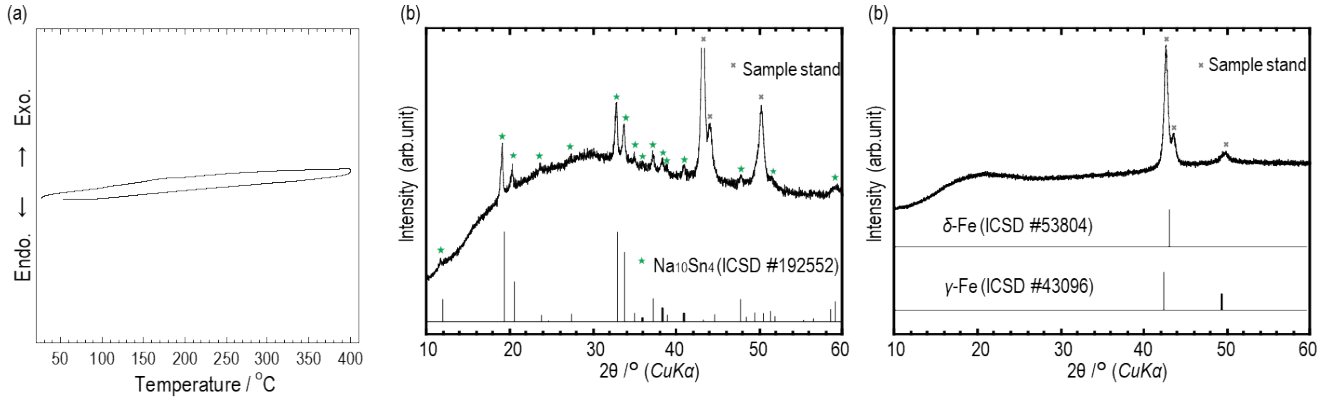


**Figure S1.** (a) DTA curve and (b) its post-measurement XRD pattern of $Na_{10}Sn_4$. (c) XRD pattern of the sample stand only. The peak of the sample stand corresponds to the iron of the foundation.

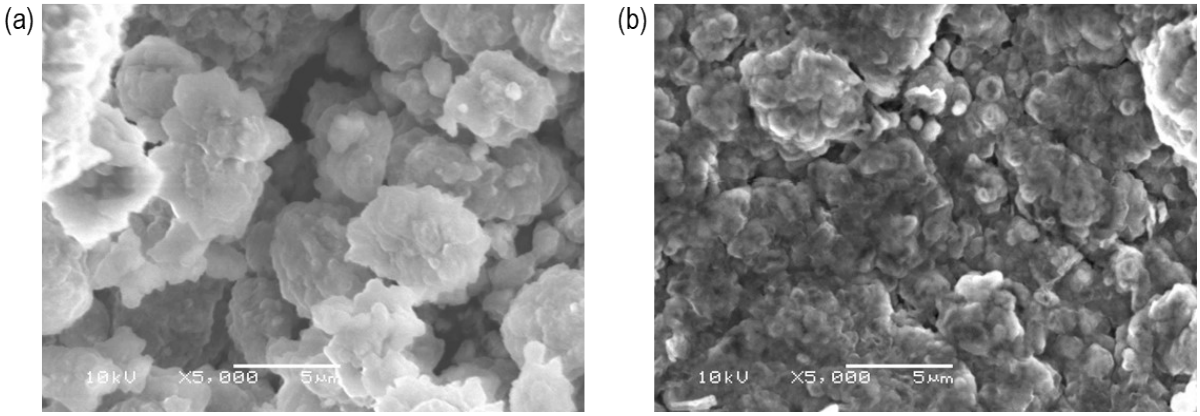


**Figure S2.** SEM images of (a) $Na_{10}Sn_4$ sample powders and (b) cross-section of a $Na_{10}Sn_4$ sample pellet.

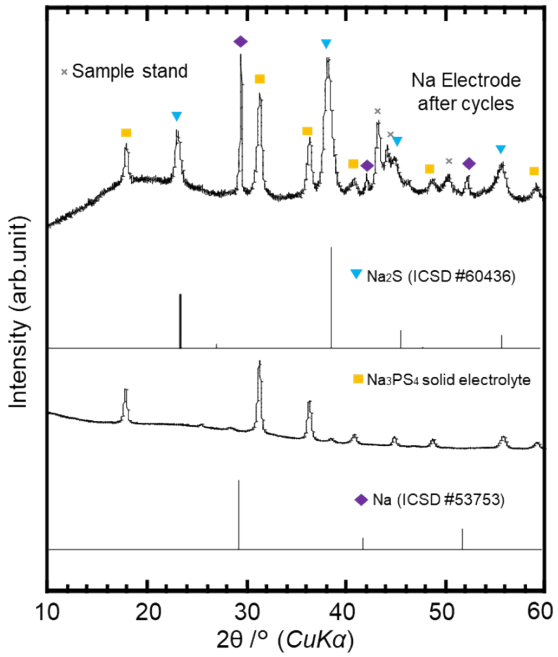


**Figure S3.** XRD pattern of Na metal electrode after constant-current cycling test. Corresponding ICSD data and electrolyte patterns are included for attribution.

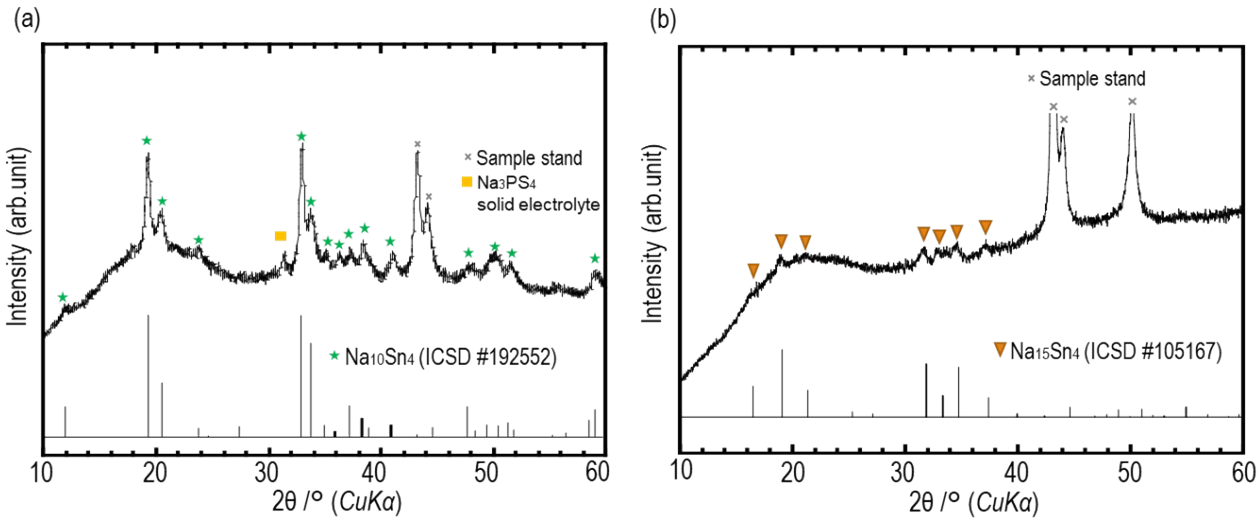


**Figure S4.** XRD pattern of Na-Sn alloy electrodes ((a) $Na_{10}Sn_4$, (b) $Na_{15}Sn_4$) after constant-current cycling test. Corresponding ICSD data are included for attribution.

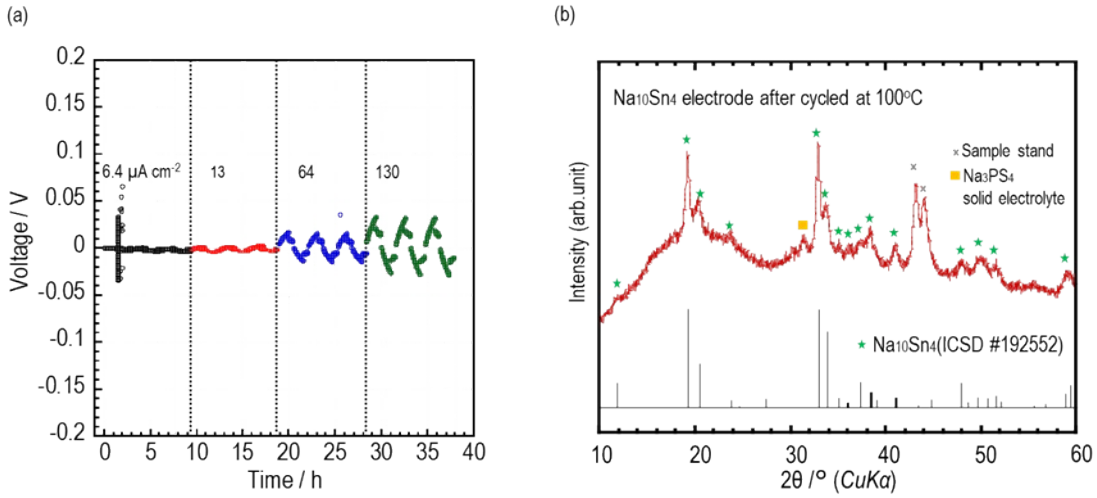


**Figure S5.** (a) Constant-current cycling test results of $Na_{10}Sn_4$ electrode at 100 ℃ and (b) XRD pattern after the test.

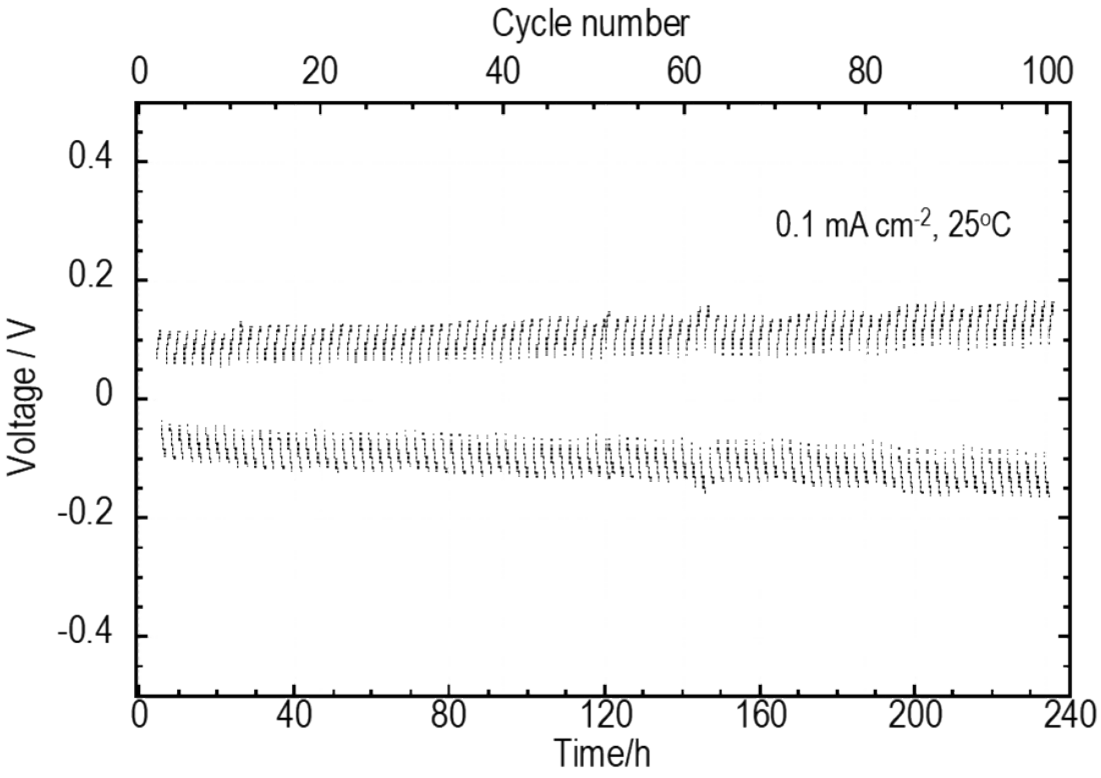


**Figure S6.** Long-term cycling test results of all-solid-state $Na_{10}Sn_4$ symmetric cell at a current density of 130 μA $cm^{-2}$ and temperature of 25 °C.

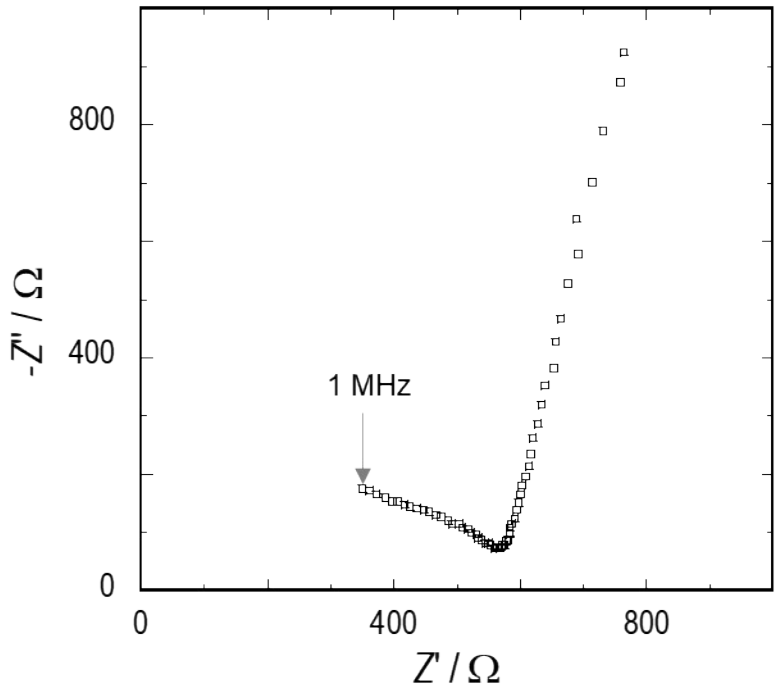


**Figure S7.** AC impedance plots of $Na_3PS_4$ solid electrolyte layer only.

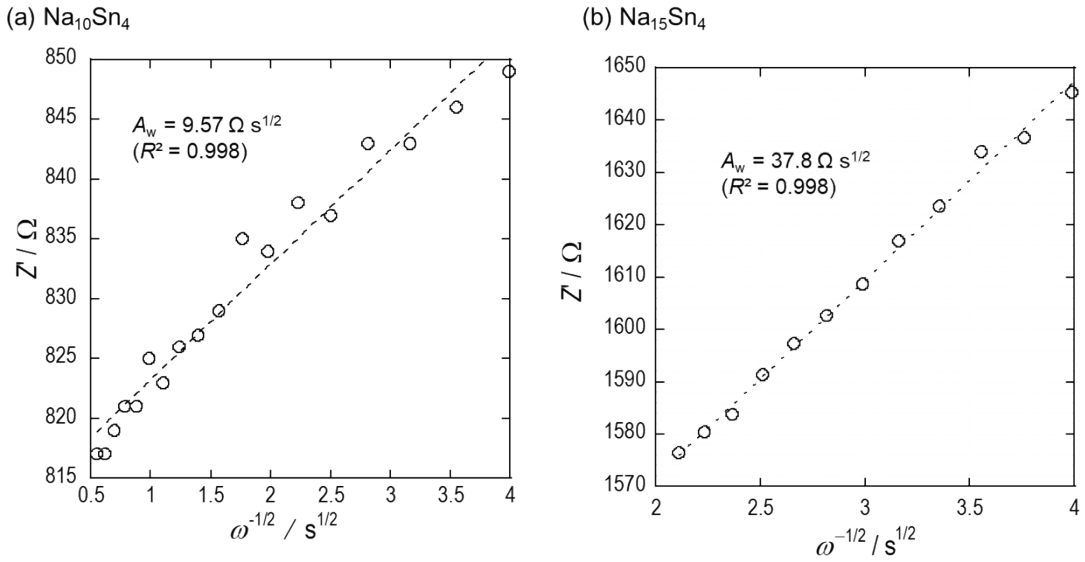


**Figure S8.** Inverse square root of angular frequency $\omega^{-1/2}$ vs. real resistance $Z'$ at the low-frequency linear part of the AC impedance plots for (a) $Na_{10}Sn_4$ and (b) $Na_{15}Sn_4$ electrodes after the charge-discharge process in an all-solid-state symmetric cell. The slope corresponds to the Warburg coefficient related to the diffusion-derived resistance.

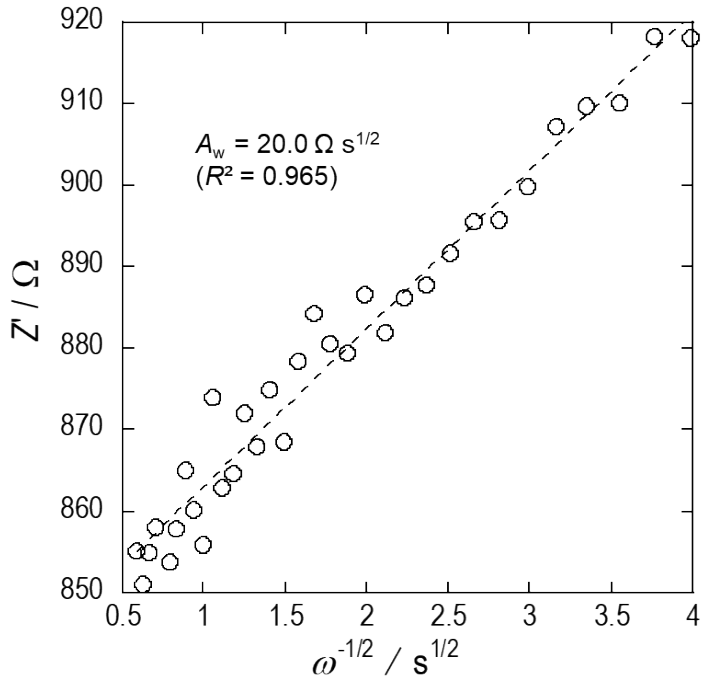


**Figure S9.** Inverse square root of angular frequency $\omega^{-1/2}$ vs. real resistance $Z'$ at the low-frequency linear part of the AC impedance plots for $Na_{10}Sn_4$ electrode after the discharge process in an all-solid-state symmetric cell. The slope corresponds to the Warburg coefficient related to the diffusion-derived resistance.

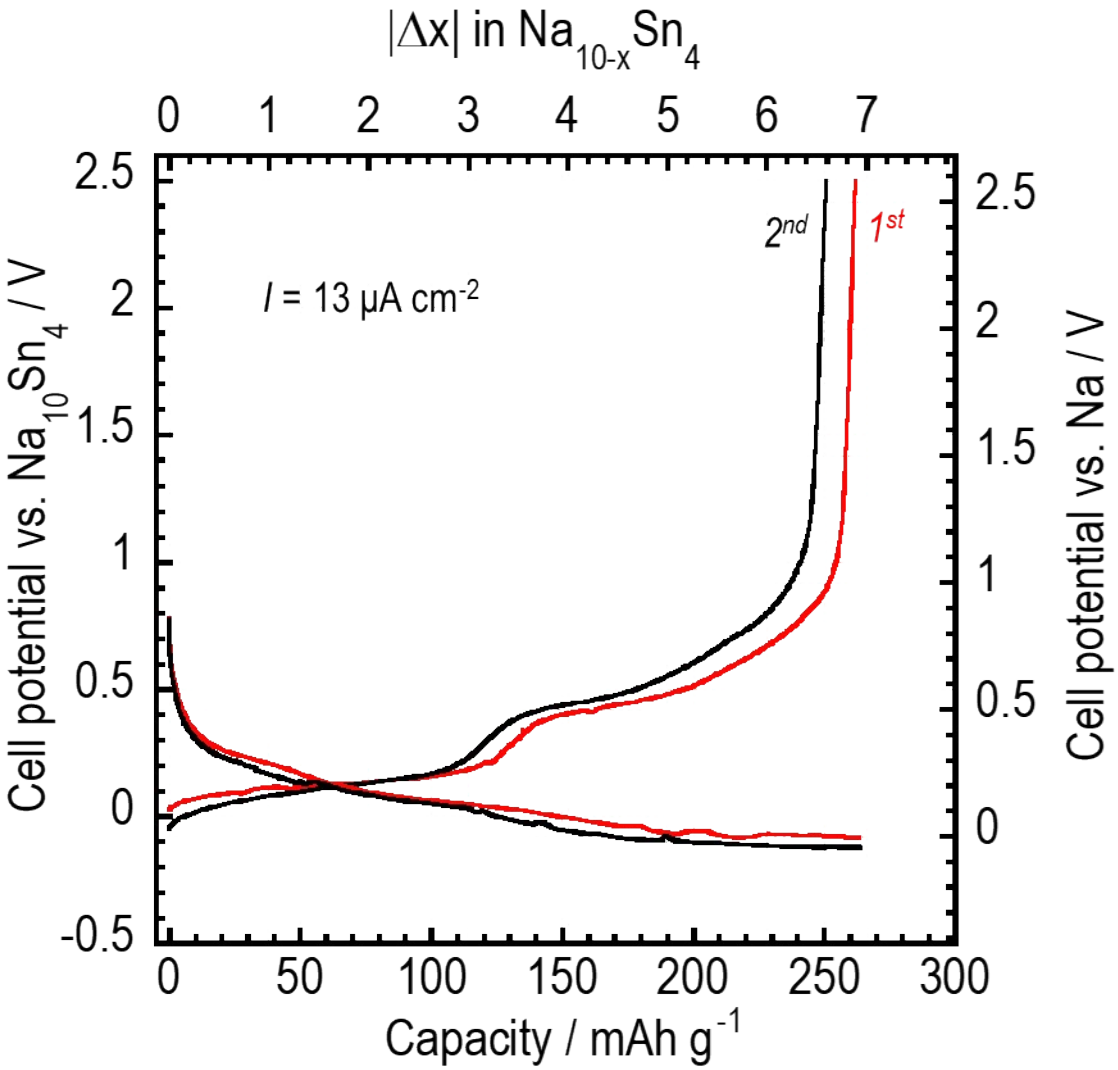


**Figure S10.** Constant-current charge–discharge measurement of a $Na_{10}Sn_4$ electrode in a $Na_{10}Sn_4$ symmetrical cell, evaluating the $Na_{10}Sn_4$ working electrode with the counter electrode in 10 times excess. The red and black lines show the charge-discharge curves at the 1st and 2nd cycles. Current density is 13 μA $cm^{-2}$ starting from the charge process. The potential for Na/Na+ on the Y2 axis is calculated as the OCV of $Na_{10}Sn_4$ (0.13 V vs $Na/Na^+$).

Na desorption was observed during charging in $Na_{10-x}Sn_4$, corresponding to an x of approximately 7, indicating reversible discharge with a capacity of 264 mAh $g^{-1}$. This reversible capacity is comparable to that of hard carbon, which is currently the leading anode material for sodium-ion secondary batteries. In addition, the low operating potential and absence of an electrolyte in the composite electrode indicate that the $Na_{10}Sn_4$ electrode may also be a high-energy-density anode.

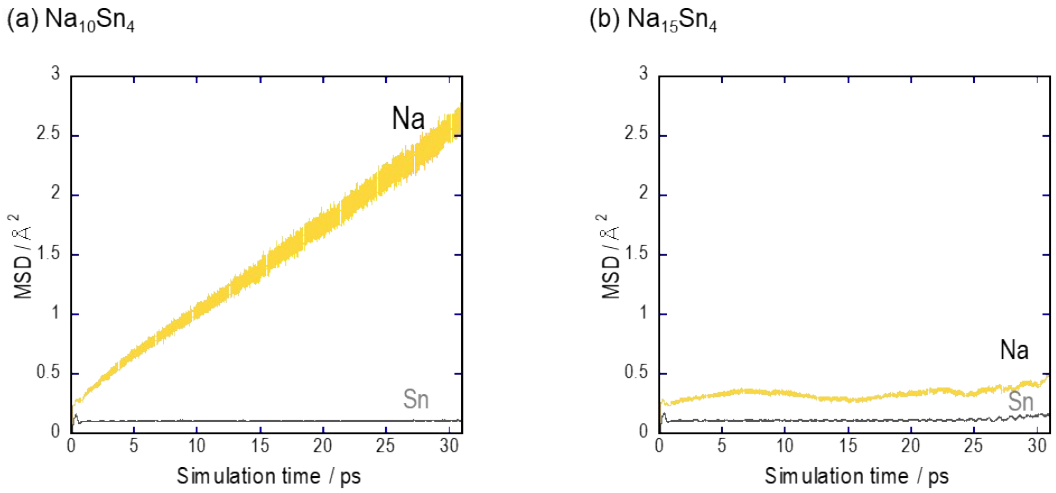


**Figure S11.** Time dependence of MSD for (a) $Na_{10}Sn_4$ and (b) $Na_{15}Sn_4$ in DFT–MD calculations at temperature 298 K.

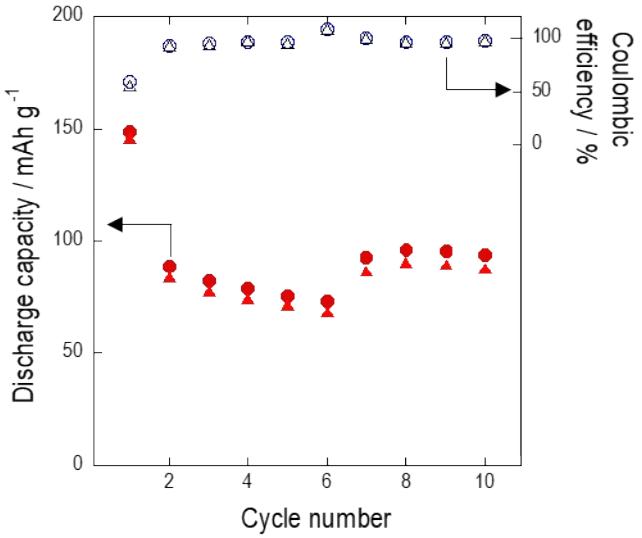


**Figure S12**. Charge–discharge cycle characteristics of the all-solid-state $Na^+$ batteries with a $Na_{10}Sn_4$ or $Na_{15}Sn_4$ anode and $TiS_2$ cathode. Circles and triangles represent data for the $Na_{10}Sn_4$ and $Na_{15}Sn_4$ anode, respectively. The $TiS_2$ cathode is a mortar mixture with $Na_3PS_4$ glass ceramics (mixture ratio $TiS_2$:$Na_3PS_4$ = 40:60 wt%). The current density and cutoff potential are 64 μA cm$^{-2}$ and 1.8–3.1 V vs Li/$Li^+$, respectively.

**Table S1.** Wykoff position of $Na_{10}Sn_4$ crystal.

| Wykoff position of $Na_{10}Sn_4$ crystal | Site | x | y | z | Occ. |
|---|---|---|---|---|---|
| Na0 | 6c | 0 | 0 | 0.21273 | 1 |
| Na1 | 6c | 0 | 0 | 0.35261 | 1 |
| Na2 | 3b | 0 | 0 | 0.5 | 1 |
| Sn3 | 6c | 0 | 0 | 0.06621 | 1 |

Space group: R$\bar{3}$m

**Table S2.** DFT-calculated relative energy values after one Na removal for each Na site in the $Na_{10}Sn_4$ supper cell.

| Na removal site | Relative energy value after one Na removal / meV |
|---|---|
| 3b | -2.25 |
| 6c | 0 |
| 6c | -23.47 |